Divergent Circulations during the Onset of the 1978–79 Australian Monsoon

N. E. DAVIDSON, J. L. MCBRIDE AND B. J. MCAVANEY

Australian Numerical Meteorology Research Centre, Melbourne, Victoria 3001, Australia

(Manuscript received 3 August 1983, in final form 11 May 1984)

ABSTRACT

Large scale numerical analyses of divergence and the divergent component of wind are examined at two levels in the lower and upper troposphere. The synoptic sequence studied includes the onset of the Southern Hemisphere summer monsoon. Comparison with satellite-observed cloudiness leads to the conclusion that the analyzed *patterns* of divergence contain synoptically realistic meteorological information. There seems to be virtually no information, however, in the day-to-day *changes in magnitude* of analyzed divergence in the lower troposphere, and only a weak signal in the upper troposphere.

The divergent wind analyses reveal the Intertropical Convergence Zone (ITCZ) to be a readily identifiable feature on individual days, and its location to be both vertically consistent and coincident with the satellite-observed cloud. Two days prior to monsoon onset the analyzed ITCZ moves poleward by 8° latitude. Monsoon convection exists at the intersection of Northern and Southern Hemisphere Hadley cells; it is well removed from the upward branch of any east–west Walker circulations in this situation.

The concept of a *divergent surge* is introduced to denote vertically consistent divergent circulations extending over distances greater than 20° latitude. This concept is shown to be useful in the physical interpretation of the role of the Southern Hemisphere subtropics in the triggering of monsoon onset. Use of the concept is also helpful in relating the day-to-day changes in tropical convection to simultaneous changes in location and intensity of (mean sea level) subtropical high pressure cells in both hemispheres.

In addition, solutions for the divergent component of wind calculated over a limited domain are compared with solutions calculated over a sphere.

1. Introduction

In an earlier paper (Davidson *et al.*, 1983, hereafter referred to as DMM), a case study was presented of the onset of the Southern Hemisphere summer monsoon at longitudes near Australia during the year of the Global Weather Experiment and its subcomponent, the Winter Monsoon Experiment (Winter MONEX). Davidson *et al.* showed that organized synoptic scale convection north of the Australian continent, as determined from satellite cloud imagery, had a sudden beginning on 26 December 1978. They defined that date as the onset of the Australian summer monsoon for that year and documented the three-dimensional structure of the troposphere during a sequence of eight days including the onset date. Using the meridional component of wind derived from large scale numerical analyses, they inferred that the monsoon convection existed in the upward branch of two linked Hadley cells, one from each of the Northern and Southern Hemispheres.

By definition, the Hadley cell exists solely in the divergent component of wind; hence the above results prompted this paper which is a study of the large scale fields of the horizontal component of divergence for the same period. The structure of the large scale divergence fields in the tropics was first studied by Krishnamurti (1971) and Krishnamurti *et al.* (1973), who derived velocity potential fields averaged, respectively, over the Northern and Southern Hemisphere summer seasons. They demonstrated that on this time scale the divergent circulations over the Asian monsoon longitudes are dominated by one large area of velocity potential maximum which is maintained by meridional "Hadley" circulations to the north and south and zonal "Walker" circulations to the east and west. The usefulness of these concepts on the shorter "day-by-day" time scale, and of the related concept of the intertropical convergence zone, has not previously been investigated. This constitutes one of the aims of this study.

Traditionally, diagnostic studies of atmospheric motions on this time scale have relied on indirect determinations of divergence through "omega" and "balance" equations (for example, see Krishnamurti, 1968 and Daggupaty and Sikka, 1977). This is largely due to the difficulty of directly measuring divergence using observations from single stations and to the extreme sensitivity of such measurements to errors in the wind observations. This sensitivity is discussed in standard meteorological texts (e.g., Holton, 1972). It would be expected that less sensitive values of divergence can be obtained using area-averaged wind values as obtained from a numerical analysis grid. This expectation was qualitatively verified in recent diagnostic studies by DMM and Davidson and

McAvaney (1981). These authors found that in the tropics synoptic scale regions of convective activity appeared as areas of low-level convergence beneath areas of upper-level divergence. Conversely, synoptic scale cloud-free regions correlated with low-level divergence and upper-level convergence. Indications are, therefore, that there is some useful information in the numerically-analyzed divergence fields. There has been no quantitative assessment, however, of the level of accuracy of this information. Such an assessment is another aim of this paper.

On the basis of their data analysis, DMM hypothesized that the trigger mechanism responsible for the onset of large scale monsoonal convection during Winter MONEX lay in the synoptic evolution of the individual cells making up the Southern Hemisphere subtropical high pressure belt. The work of a number of other authors (Williams, 1979; Lim and Chang, 1981; Lau and Lim, 1982; Murakami and Sumi, 1982a) indicates that Southern Hemisphere monsoon activity also responds directly to fluctuations in the Northern Hemisphere subtropical belt. A third aim of this paper is, accordingly, to use the large scale analyses of divergent wind to further investigate the forcing of tropical convection by the subtropics of both hemispheres.

The three aims of the paper are thus:

1) To provide a quantitative assessment of the level of accuracy of kinematically derived divergence fields obtained from an optimum interpolation analysis scheme and the Winter MONEX data set (Section 2).

2) To investigate the concepts of the ITCZ and Hadley and Walker circulations on the day-to-day time scale (Section 3).

3) To investigate the forcing of tropical convection by the subtropics of both hemispheres (Section 4).

A problem that plagues all work on the decomposition of wind fields into divergent and rotational components is the specification of lateral boundary conditions. This paper also includes some results of general interest in this context. In particular, a comparison is made of solutions for the divergent component of wind calculated over a limited domain with solutions calculated over a sphere.

2. Divergence fields

The veracity of divergence fields determined kinematically from analyzed wind components is strongly dependent on the analysis method and on the density and quality of wind observations. Over the tropical oceans, and particularly in the Southern Hemisphere, the distribution of upper air stations is sufficiently sparse to preclude the accurate determination of divergence at middle tropospheric analysis levels. During Winter MONEX, however, the conventional data base was supplemented by a large number of satellite cloud winds from the University of Wisconsin, and obtained using imagery from the earth-synchronous satellites GMS-1 and GOES-1. The satellite wind observations are concentrated in the very low and the very high levels of the troposphere. Consequently, in this study analyses are presented at only two levels, 950 and 200 mb—representative of the lower and upper troposphere, respectively.

The data density is illustrated in Fig. 1, which shows the observations available to the analysis program at these levels for 0000 GMT 24 December 1978. The analysis method is three-dimensional univariate optimum interpolation as described by Davidson and McAvaney (1981). The vertical correlation functions allow the effective use of observations falling as far as 1500 m from the nominated analysis level. The 950 mb analysis also makes use of surface land and ship reports corrected for friction. In the optimum interpolation technique, the satellite-derived winds receive less weight than those from rawinsondes, mainly because of the severe height assignment problem. This relative weighting is of particular importance in the upper-level high wind-shear zones at middle latitudes, and has the effect of decreasing incompatibilities between the data types.

In Fig. 1, the region most deficient in observations is the Indian Ocean to the west of Australia. The data base here consists almost entirely of satellite winds and ship reports. It is hence variable in observation density from day to day. Over the rest of the analysis domain the data distribution seems sufficient to monitor daily changes in synoptic scale divergence. It remains to be determined whether the observations and analysis method are sufficiently accurate for this divergence field to be representative of that in the atmosphere.

The infrared satellite images for the monsoon onset situation studied by DMM are shown in Fig. 2. Images are shown at 0000 GMT 22 December 1978, 2100 23 December and 0000 26 December. The situation is described in detail by DMM. For the present purposes the major features are as follows. A semicontinuous line of tropical convection, representing the planetary scale ITCZ, is seen stretching from west to east across the center of all three photographs. On 22 December its mean latitude is closer to the equator. During the following four days there is a gradual shift southward, so that on 26 December the latitude of the main cloud band is approximately 8°S. There is also a dramatic change taking place in the overall intensity of the tropical convection, with only sparse and scattered cloud on the first two images but widespread dense areas of cloud on the third.

Divergence fields at 950 and 200 mb for the same three date–times are shown in Fig. 3. To simplify the presentation, the only coastline shown is that of the

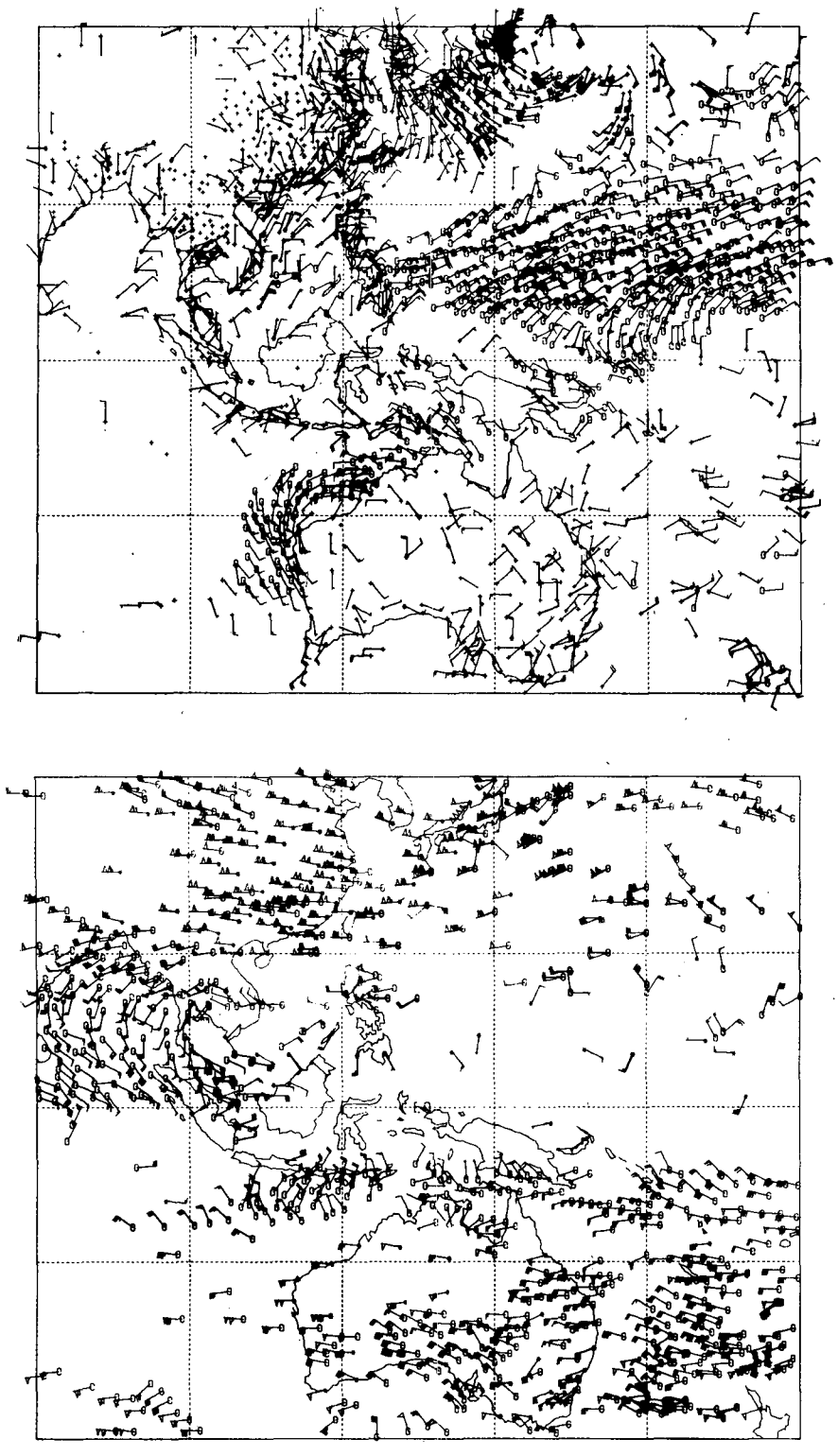

FIG. 1. Observational data base available to the numerical analysis below 900 mb (top) and within 25 mb of 200 mb for 0000 GMT 24 December 1978. Observations designated by stars are rawinsondes, open circles are aireps and satellite cloud winds, and crosses are surface synoptic data.

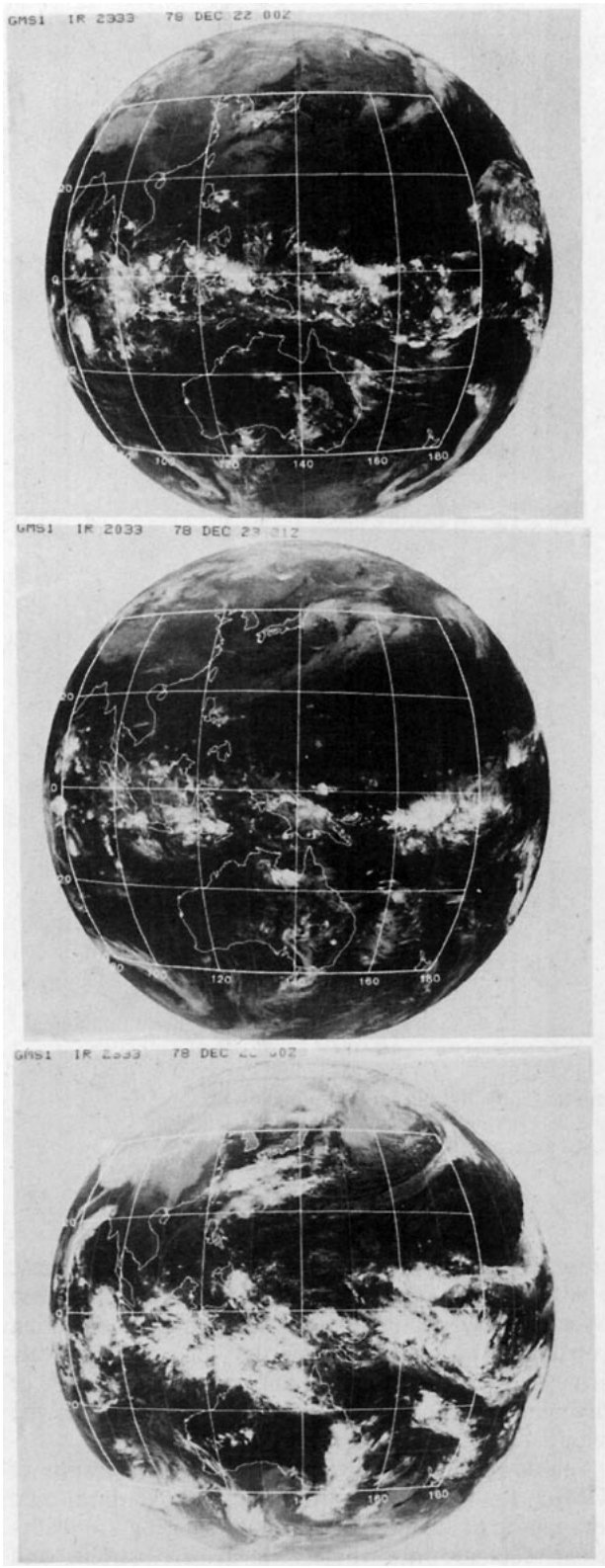

FIG. 2. Infrared satellite cloud imagery for 0000 GMT 22 December 1978 (top), 2100 23 December (center) and 0000 26 December (bottom).

Australian continent. Also, for simplification only selected contours are shown. The left-hand column is divergence at 950 mb. Contours are for divergence values of zero and -0.5×10^{-5} s^{-1}, and shading denotes areas with convergence greater than the latter value. The right-hand column is 200 mb divergence, showing the zero contour and shaded areas of divergence greater than $+1.0 \times 10^{-5}$ s^{-1}.

The general character of the patterns agrees well with the satellite cloud images in Fig. 2. The ITCZ is represented as a band of convergence at 950 mb overlain by a band of divergence at 200 mb. These bands move southward over the analysis period, also in correspondence with the satellite cloudiness.

Both the vertical consistency of the large scale divergence patterns and their correspondence with the cloudy and cloud-free areas are particularly marked between 20°N and 20°S. For example, on 24 December (middle row of Fig. 3) the cloud near 5°S, 160–180°E appears as a low-level convergence maximum and as an upper-level divergence maximum. Similar comments hold for the cloud area on the same day near 5°S, 120°E.

Hence the overall impression gained from inspection of Fig. 3 is that there is information content in the large-scale patterns of analyzed divergence. Turning attention now to the actual *magnitudes* of divergence, the results are not as good. The major feature of the satellite imagery in Fig. 2 is the large increase in the amount of tropical cloudiness occurring on 26 December. No reflection of this increase appears on the divergence maps of Fig. 3; neither an increase in the area of upper- (lower-) level divergence (convergence), nor an increase in the shaded regions of divergence (convergence) maxima.

A more objective assessment of the variation in magnitude of divergence is obtained from consideration of Fig. 4. This shows a time series over nine days of the area-average divergence between 100 and 150°E, and over a 20° latitude band spanning the main zone of tropical cloudiness on each day. The figure reveals no obvious trend in divergence at the 950 mb level. At 200 mb it appears that an increase has occurred five days prior to monsoon onset, so there may be some information in the magnitudes of the analyzed divergence at this upper level. The increase is not apparent in the patterns in the right-hand column of Fig. 3 because it has already taken place at the time of the earliest analysis in that figure.

Time-series of divergence over a similar region but for a longer period have been presented by Murakami and Sumi (1982a). Figure 2 of their paper shows an increase of 200 mb divergence between 0 and 10°S occurring in late December and peaking to a maximum on about 25 December.

The overall picture which emerges from the results of this section is that there is considerable information

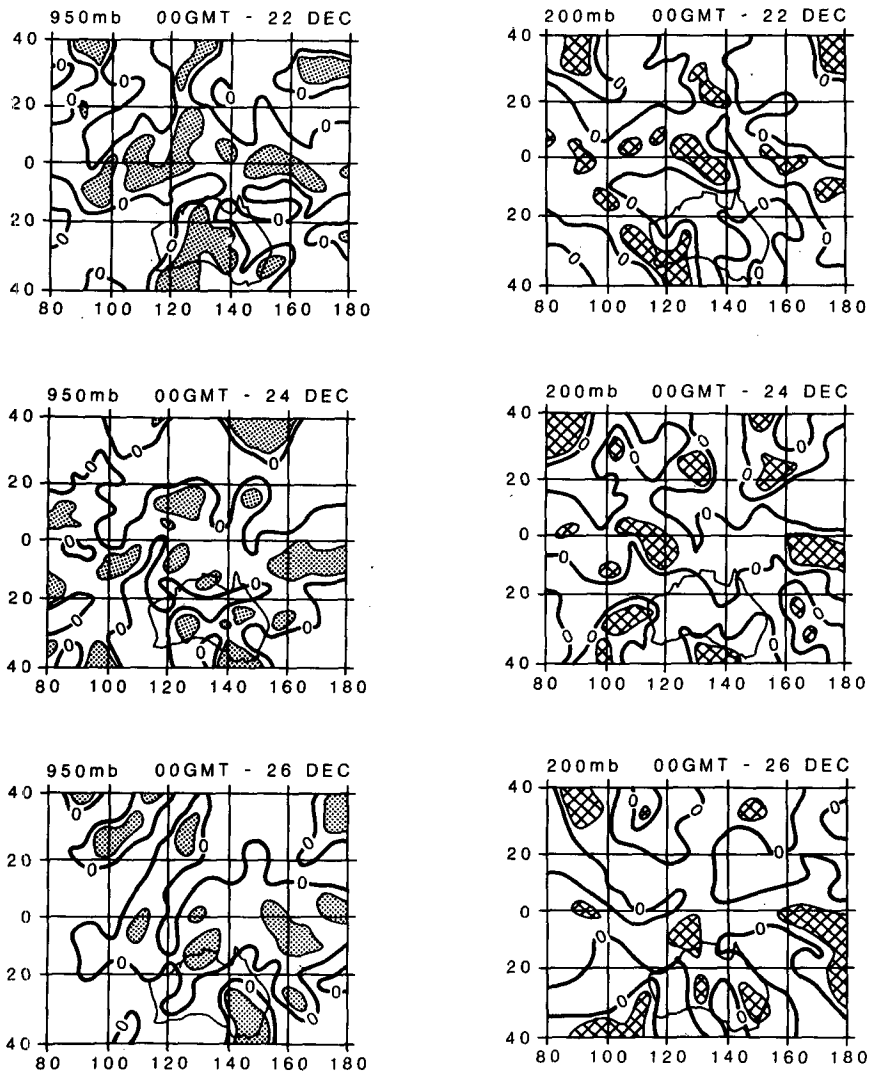

FIG. 3. Derived divergences (10^{-5} s^{-1}) at 950 mb (left) and 200 mb (right) for 0000 GMT 22 December 1978 (top), 24 December (center) and 26 December (bottom). Stippled areas at 950 mb are values less than -0.5×10^{-5} s^{-1}. Hatched areas at 200 mb are values greater than 1.0×10^{-5} s^{-1}.

in the patterns of analyzed divergence and in the locations of the areas of maximum divergence and convergence. There seems to be virtually no information in the day-to-day *changes in magnitude* of analyzed divergence at the analysis level in the lower troposphere. At the upper tropospheric level there is a weak signal corresponding to the increase in cloud used to define monsoon onset. The time-consistent upper-level divergence changes seem to occur, however, prior to and over a longer time scale than the changes in convection.

The presence of a stronger signal at upper levels than at lower levels is partially explained by the vertical distribution of divergence in the convectively enhanced regions. As shown by DMM (and for other tropical regions of the word by McBride and Gray, 1980), the convective weather system is characterized by a deep layer of relatively small convergence which is balanced by a shallow upper-level layer of relatively large divergence. This resultant smaller magnitude of divergence at lower tropospheric levels increases the significance of noise in the analyses.

These results shed light on some of the results of DMM for this same situation. They monitored changes in divergence averaged over a geographically-fixed rectangle immediately north of Australia, and found a large increase in low-level convergence and upper-level divergence prior to monsoon onset. The results of this study reveal that this effect is due entirely to a southward shift into their rectangle of

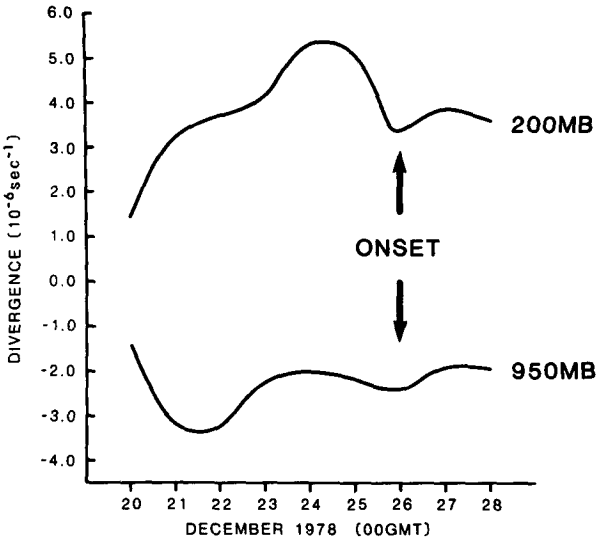

FIG. 4. Time series of 950 and 200 mb divergences (10^{-6} s^{-1}), area-averaged between 100 and 150°E and over a 20° latitude band spanning the main zone of tropical cloudiness on each day.

the ITCZ as it appears in the divergence analyses. There is no contribution from any change in the analyzed magnitude of the ITCZ.

3. Divergent circulations

The Hadley and Walker circulations are defined here as closed cells in the Y–Z and X–Z planes, respectively. Accordingly, their manifestation in the horizontal plane is totally in the divergence component of wind. This is obtained by standard techniques (see, for example, Krishnamurti, 1971; Krishnamurti *et al.* 1973) involving the solution of the following system of equations over the analysis domain:

$$\mathbf{V} = \mathbf{V}_\psi + \mathbf{V}_\chi = \mathbf{k} \times \nabla\psi + \nabla\chi, \quad (1)$$

$$\nabla^2\psi = \xi, \quad (2)$$

$$\nabla^2\chi = D, \quad (3)$$

where $\mathbf{V}$ is the horizontal wind vector; $\mathbf{V}_\psi$ and $\mathbf{V}_\chi$ are the rotational and divergent components of the horizontal wind, respectively; ψ is the streamfunction, χ the velocity potential; ξ the vertical component of vorticity and D the horizontal component of divergence.

To solve the system over a limited domain, boundary values must be specified for ψ and χ. Following Sangster (1960) and Shukla and Saha (1974), χ is set to zero on the boundaries, and boundary conditions for ψ are generated using the solution of (3) and the component of the analyzed wind parallel to the boundary. A measure of the accuracy of the solution procedure is obtained by using the solutions of (2) and (3) to reconstruct the total wind in (1). The root-mean-square error between this and the analyzed wind is represented in Table 1 for the subdomain starting four grid points in from each boundary.

It should be noted, however, that these small errors do not guarantee the correct partitioning of the wind into rotational and divergent components. This limitation will be discussed later in the section.

Figures 5 and 6 show vector arrow plots of the resultant divergent component of wind at the two analysis levels at 0000 GMT 22, 24 and 26 December 1978. The shaded areas denote divergent wind magnitudes greater than 4 m s^{-1} in Fig. 5 (950 mb) and 6 m s^{-1} in Fig. 6 (200 mb). The major feature in both figures is a distinct east–west discontinuity separating northerly from southerly divergent winds (marked by a hatched line). This line is conceptually equivalent to the intertropical convergence zone which separates the converging northerly trades from the Northern Hemisphere and the southerly trades from the Southern Hemisphere. The line will henceforth be referred to as the DITCZ (diagnosed intertropical convergence zone). The lower-level flow to the north of the DITCZ is northerly (Fig. 5), while at the upper level (Fig. 6) it is southerly. Accordingly, this region is the Northern Hemisphere winter Hadley cell. Similarly, the Southern Hemisphere summer Hadley cell can be seen immediately south of the DITCZ. The main branches of each cell on each day are designated on the figures by thick arrows. These will be defined objectively later in this section.

The vertical consistency in these divergent circulations is remarkable, with the 200 mb DITCZ approximately overlying that at 950 mb, and the main northerly and southerly flows also overlying each other. The joint concepts of the ITCZ and Hadley cell were originally developed to understand and explain features of the long term mean and zonally averaged global flow (see Lorenz, 1969). Figures 5 and 6 demonstrate that over the monsoon region the concepts are equally applicable to the flow on a single day and that these features can actually be identified through the performance of a divergent wind analysis.

Further inspection of Figs. 5 and 6 reveals that the divergent flow during this particular monsoon situation is dominated over Australian longitudes by the two (Northern and Southern Hemisphere) Hadley cells. Substantial east–west (or Walker) circulations appear only near the eastern and western boundaries of the analysis domain, where the χ solution is unreliable and influenced by boundary effects.

TABLE 1. Root-mean-square error between total wind from (1) and the analyzed wind.

Pressure level (mb)	rms U error (m s^{-1})	rms V error (m s^{-1})
950	1.2	1.1
200	2.7	2.3

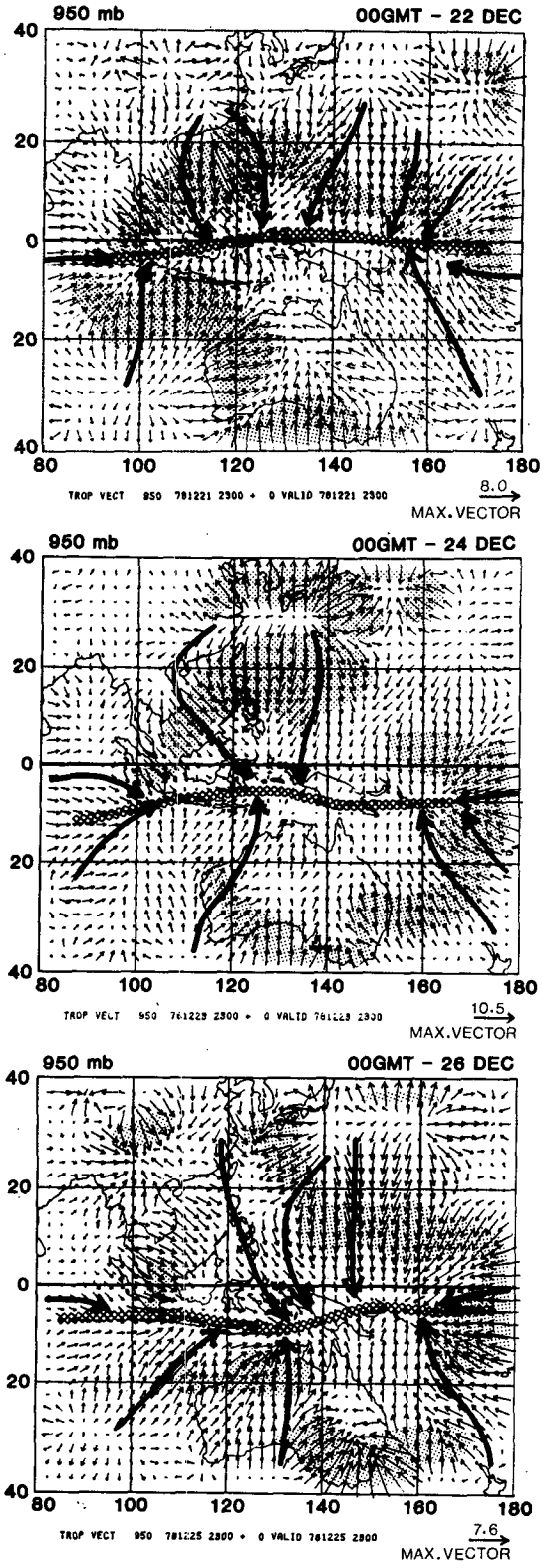

FIG. 5. Diagnosed divergent wind component analysis (m s^{-1}) at 950 mb for 000 GMT 22, 24 and 26 December 1978. Shaded areas are winds greater than 4 m s^{-1}. Thick arrows denote the vertically-consistent main branches of the divergent circulations as defined in the text.

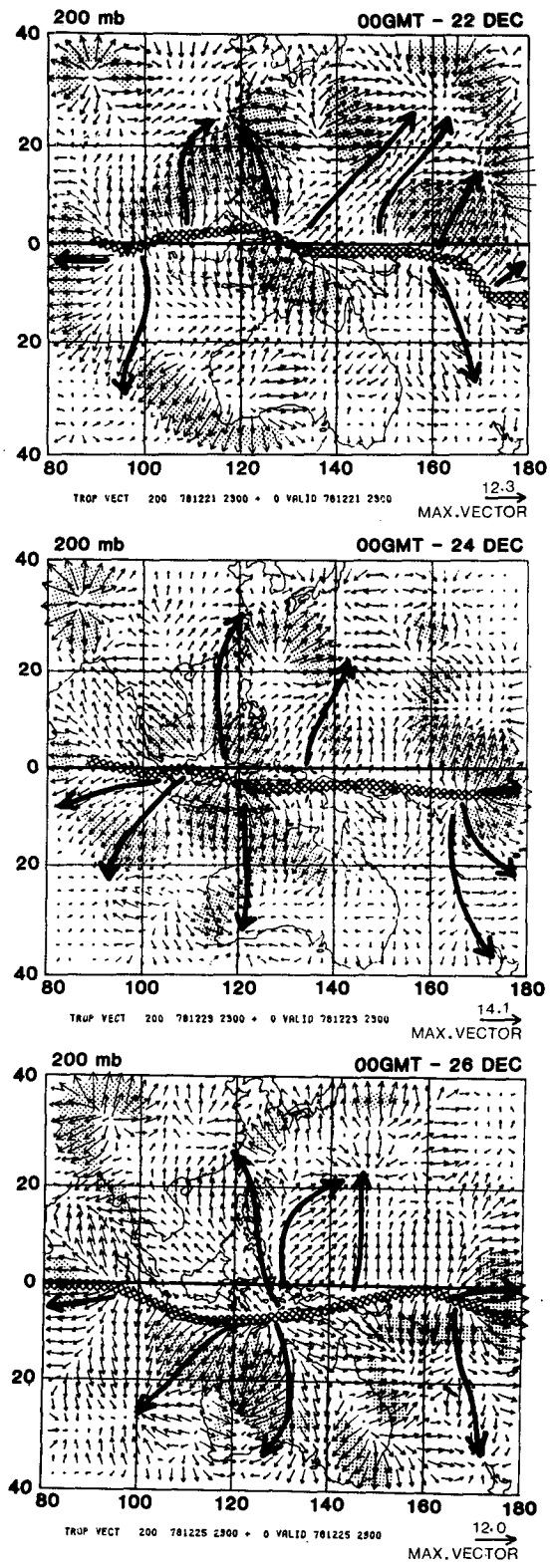

FIG. 6. As in Fig. 5 but at 200 mb. Shaded areas are winds greater than 6 m s^{-1}.

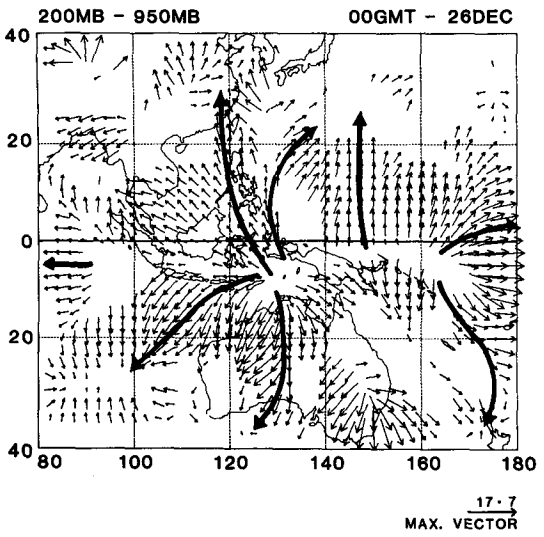

FIG. 7. Vector wind arrow chart showing the 200 mb minus the 950 mb divergent wind (m s^{-1}). Only those grid points where the upper and lower divergent winds differ in direction by between 135 and 225° are plotted.

The location of the DITCZ coincides with the axis of the main tropical band in Fig. 2, and it moves southward with the cloud band as the large scale onset of monsoon convection takes place.

The heavy arrows in Figs. 5 and 6 are drawn to schematically represent the main branches of the vertically consistent divergent circulations. These were computed by producing charts showing the divergent wind only at those grid points where the upper and lower divergent winds differ in direction by between 135 and 225°. An example of such a chart is shown in Fig. 7. Heavy arrows (henceforth for convenience referred to as "divergent surges") were drawn on the chart through all continuous flows extending for more than 20° latitude. While there is some arbitrariness in this definition, the resultant divergent surges plotted in Figs. 5 and 6 seem to represent reasonably well the main circulations in these figures. This is substantiated by careful comparison with Fig. 2 which reveals a good correspondence between the tropical ends of the divergent surges and the locations of the main centers of convective activity. The divergent surges will be used extensively in the following to relate the divergent wind maps to the synoptic evolution of the flow as documented by DMM.

Some caution is necessary in the interpretation of the above results. The divergent wind maps have been derived by the solution of Eq. (3) over a limited domain. The solution under such circumstances is not unique. For example, the addition of any function $Ax + By + C$, where A, B and C are constants, to the velocity potential χ will also yield a solution to Eq. (3). Thus the divergent wind maps can be modified by the addition of any constant wind vector (A, B), which has the effect of moving the location of features such as the DITCZ.

The current solution is obtained by setting χ constant along the boundaries. This has been demonstrated by Sangster (1960) to minimize the kinetic energy of the divergent wind over the domain. This procedure has also been used by other workers interested in the locations of peaks in the χ fields (e.g., Krishnamurti, 1971; Murakami and Sumi 1982b).

Since there is no *a priori* information on the value of χ along the boundary, there is no satisfactory solution procedure for a closed domain. To further investigate the effect on χ and V_χ of the computational method and imposed boundary conditions, we used FGGE IIIB data from the European Centre for Me-

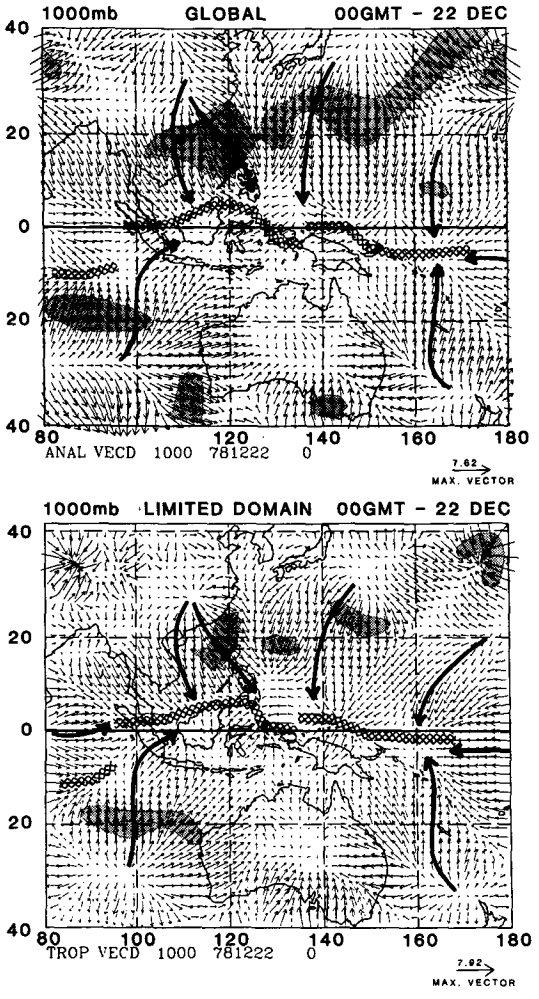

FIG. 8. Diagnosed divergent windfield at 1000 mb for 0000 GMT 22 December 1978 from the ECMWF global analysis, showing (top) the relevant portion of the solution obtained from a global calculation and (bottom) the solution obtained over a limited domain using the χ constant boundary condition. Shaded areas are winds greater than 4 m s^{-1}. Thick arrows denote the vertically consistent main branches of the divergent circulations as defined in the text.

dium Range Weather Forecasts (ECMWF) to compare $\mathbf{V}_\chi$ solutions obtained from limited area and global data sets of the same analysis. First, the ECMWF global analysis for 0000 GMT 22 December 1978 was used to compute $\mathbf{V}_\chi$ on the sphere, from which the divergent windfield over the appropriate Australian sector was extracted. Details of the calculations are given in the Appendix. Second, the *total* wind analysis of the limited, Australian sector was obtained from the ECMWF global analysis, and $\mathbf{V}_\chi$ then computed using the constant boundary condition. Comparison of the results (Figs. 8 and 9) reveals the following conclusions:

1) The locations of the DITCZ and divergent surges are extremely similar for the global and limited area calculations.

2) Within 10° latitude of the boundary of the limited area calculation, the solution is often strongly affected by the imposed boundary conditions. This is most evident near the northern boundary of the 200 mb chart where the major convergent centers over China and east of Japan have been shifted southward by ~5° latitude.

3) The magnitudes of the divergent winds obtained from the limited area calculation are smaller. This result reflects the minimization of the kinetic energy of the divergent wind imposed by the boundary conditions (Sangster, 1960).

4) In the subdomain starting some 10° latitude in from the boundaries, the patterns of the derived divergent windfields are extremely similar.

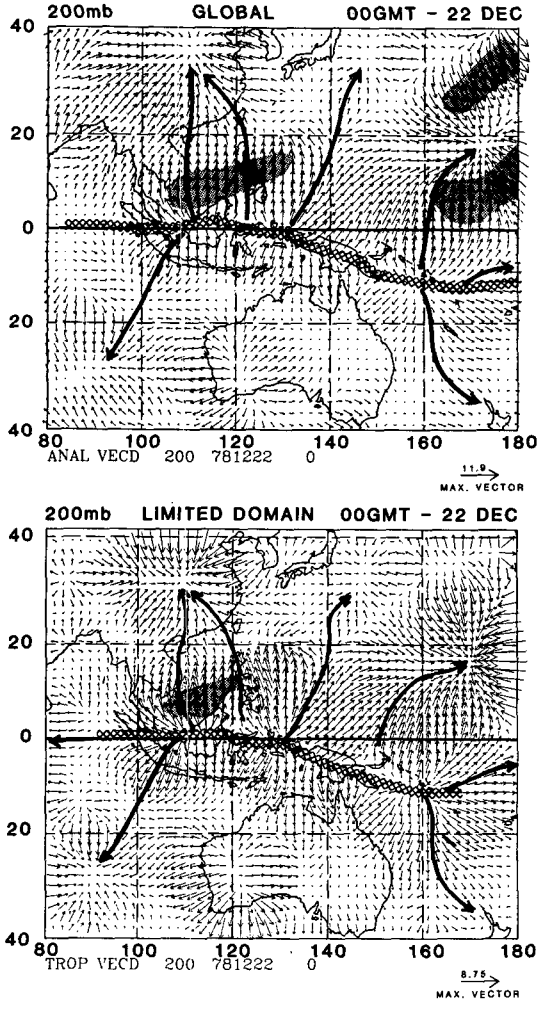

FIG. 9. As in Fig. 8 but at 200 mb. Shaded areas are winds greater than 6 m s^{-1}.

It is also informative to compare the $\mathbf{V}_\chi$ solutions from different analyses, and presumably different data bases. [It is important to note that because of the Normal Mode Initialization (NMI) used in the European Centre's system during this period, divergence and vertical motion over the tropics is considerably reduced (see, for example, Puri and Bourke, 1982). This necessarily has some adverse effects on the computed divergent windfield.] Comparison of Figs. 5, 6, 8 and 9, which show divergent windfields obtained from the different analyses, reveals the following conclusions:

1) The large scale patterns of the corresponding charts are very similar even though the magnitudes of derived divergence over the tropics differ considerably in the two analyses.

2) There are clearly small scale differences which are presumably related to data base differences, analysis system differences, the NMI method and, at the lower level, to the slightly different analysis levels.

3) There is reasonable consistency between the diagnosed locations of the DITCZ. The largest differences occur over the South Pacific where the vertical consistency of the upper- and lower-level positions of this feature appears to be more realistic in Figs. 5 and 6.

4) The locations of the divergent surges are not particularly sensitive to the analysis from which they are derived.

In summary, if we limit our attention to the larger scales inside 10° latitude from the boundaries of the analysis domain, the $\mathbf{V}_\chi$ solutions are sufficiently general to allow useful synoptic interpretation.

4. Relationships between divergent flow and synoptic features

Figure 10 shows a sequence of one-per-day mean sea-level pressure analyses finishing on the day of monsoon onset, 26 December. Superimposed are the divergent surges as defined in Section 3. To aid interpretation, it is noted that the numerical analysis scheme used in this study is univariate; hence the divergent wind analysis used to delineate the divergent

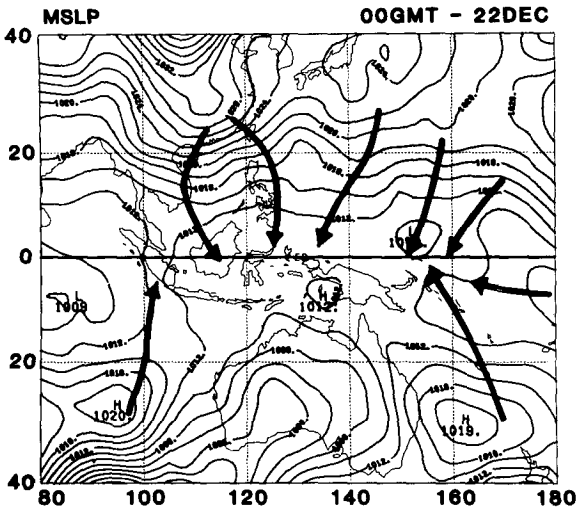

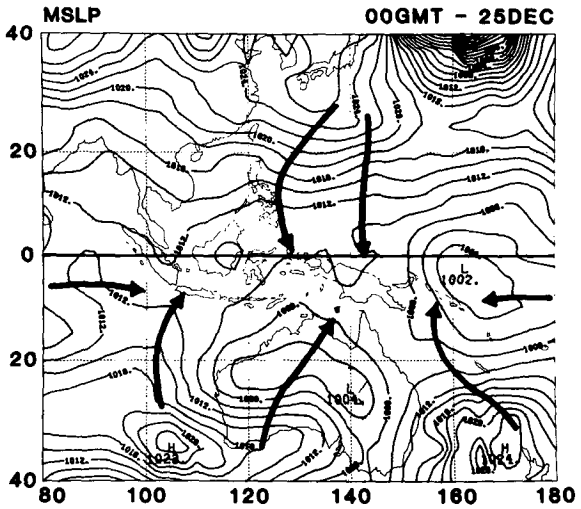

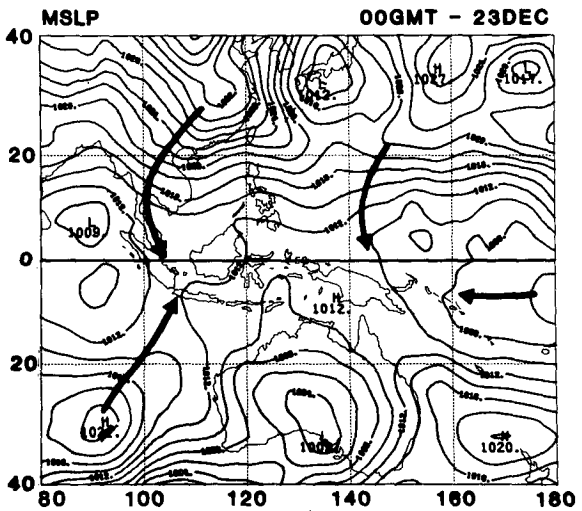

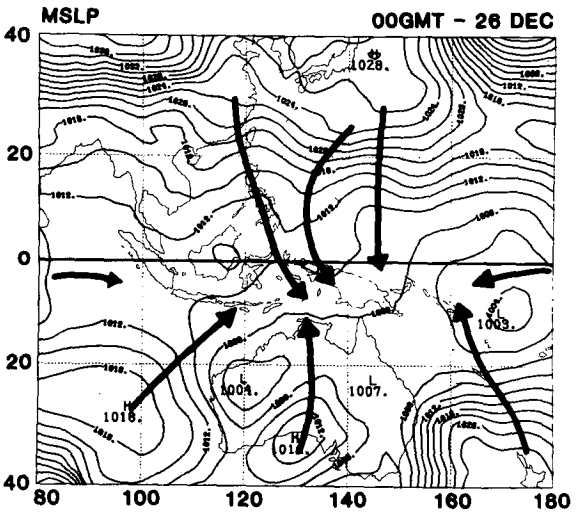

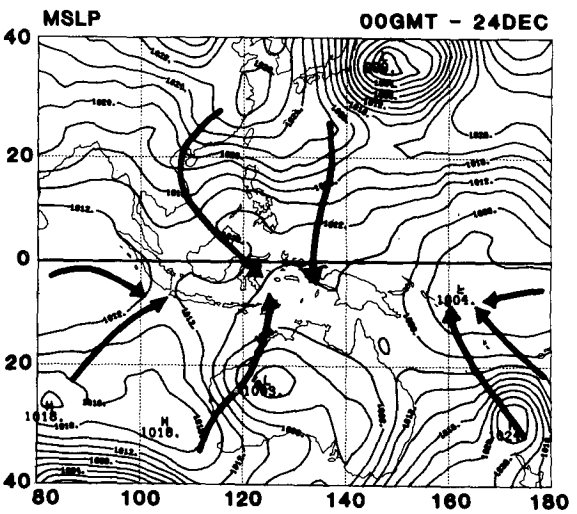

FIG. 10. Mean sea-level pressure analyses at 0000 GMT 22, 23, 24, 25 and 26 December 1978. Thick arrows denote the vertically consistent main branches of the divergent circulations as defined in the text. Contour interval is 2 mb.

surges is completely independent of the mean sea-level pressure analysis.

Inspection of Fig. 10 reveals that the day-to-day changes in the divergent surges are related to the changes in the individual high pressure cells of the subtropical ridge in both hemispheres. Each surge emanates from either a ridge or a separate high cell, and in most cases from the eastern and equatorward sector of the high cell.

The major tropical weather event occurring during the sequence is the large scale enhancement of cumulonimbus activity on 26 December. In the previous section it was shown that this event does not correspond to any increase in magnitude of analyzed divergence. It does, however, correspond to a synoptically consistent change in the locations of the divergent surges.

At the beginning of the sequence, no Southern Hemisphere divergent surges exist over Australian longitudes. In the following days the Southern Hemisphere subtropical ridge intensifies across the longitude span from 100 to 160°E, leading to the establishment of divergent surges in these longitudes. Northern Hemisphere divergent surges exist over the region throughout the sequence, so that at the time of the outbreak of convection a convergence region has been established between the surges making up local branches of the Hadley cells from both hemispheres.

The changes in intensity of the Hadley cells during the onset period have been examined using the mean meridional components of the divergent wind between 100 and 150°E, and within 25° latitude of the DITCZ. At 200 mb the general trends are for the Northern Hemisphere branch to remain steady while the Southern Hemisphere branch more than doubles in strength during the five days leading up to the outbreak of tropical convection. At the time of onset it is comparable in strength to the Northern branch. No clear trends are evident at the 950 mb level.

It is of course difficult to establish cause and effect between the subtropical ridge intensification, the strengthening of the Southern Hemisphere Hadley cell and the tropical convection. In our opinion, the fact that the ridge begins to intensify at least two days prior to the outbreak of convection suggests that, on short timescales the outbreak of tropical convection was related more to subtropical effects than to tropical events.

The interpretation of events in terms of divergent surges is still, however, suggestive rather than conclusive. This uncertainty is due to:

1) The subjectivity in definition of the surge.
2) The sensitivity of analyzed divergence to data density and measurement errors.
3) The analytical problems, discussed in the previous section, associated with the derivation of the divergent component of wind.

If this interpretation is correct, however, it has profound implications for understanding the forcing of tropical convection by the large scale flow. The divergent surges emanate from the individual high pressure cells of the mean sea-level subtropical ridge and end within the cloud clusters constituting the monsoon cloudiness. This suggests that the day-to-day variations in monsoon cloudiness are associated with, and may even respond directly to, the variations in the subtropical highs. Thus the secret to understanding (and predicting) the evolution of monsoon activity on this time scale may lie in the understanding (and prediction) of the subtropical high cells.

It is appropriate to comment on certain other aspects of the divergent surges shown in Figs. 5 and 6. Many authors have emphasized the importance of "cold surges" in the trade winds in the forcing of tropical convection (for example, Cheang, 1977; Chang *et al.*, 1979). Figures 3, 4 and 5 of DMM reveal the occurrence of two such "cold surges" during the situation studied here, one in the South China Sea on 22 December and the other along the west Australian coastline on 24 December. Divergent surges exist in these same locations at the same times. Low-level divergent wind speeds in the region are typically of the order of 6 m s^{-1}, whereas the total wind speeds are typically 15 m s^{-1}; thus, the more substantial contribution to the cold surge lies in the rotational component of wind. Also, many divergent surges appear on Figs. 5 and 6 in areas where no "rotational" cold surges exist. The relationship between the two types of surge is thus unclear and should be the subject of further investigation.

The divergent surges were defined in the previous section based on a criterion of vertical consistency in the analyses of divergent wind at 950 and 200 mb. It has been shown above that the locations of the surges are related to the high pressure cells and ridges at mean sea level. The wind analyses at the upper level (200 mb) have also been examined for correspondence between the surges and particular synoptic features. No consistent relationships are apparent, though in some cases the higher latitude ends of the surges are located near jet maxima on the eastern side of westerly troughs [similar to the situations for "cold surges" discussed by Webster (1981) and Chang and Lau (1982)].

5. Conclusions

Large scale numerical analyses of divergence and the divergent component of wind have been investigated for a sequence of five days. The sequence includes the onset of the Southern Hemisphere summer monsoon during the international monsoon experiment, Winter MONEX. The investigation concentrates on only two tropospheric levels, 950 and 200 mb.

The divergence analyses are compared with tropical upper-level cloudiness as observed on infrared satellite imagery. It is concluded that there is information content in the large scale *patterns* of analyzed divergence. However, there seems to be virtually no information in the day-to-day *changes in magnitude* of analyzed divergence in the lower troposphere and only a weak signal in the upper troposphere.

Analyses of the divergent component of wind reveal that the ITCZ is a readily identified feature on individual days, and that its location is both vertically consistent and consistent with the main areas of tropical convection. Over a period of two days leading up to monsoon onset, the ITCZ is observed to move poleward by 8° of latitude. The monsoon convection exists at the intersection of two Hadley cells, from the Northern and Southern Hemispheres. No east-west Walker circulations are present near the main areas of monsoon convective activity in this particular situation.

Vertically-consistent divergent circulations extending for more than 20° latitude distance have been denoted by the term "divergent surges." The tropical ends of the divergent surges correspond closely to the locations of the main centers of convective activity. The higher latitude ends of the surges generally emanate from the eastern and equatorward sides of high pressure cells in the mean sea level subtropical ridges of both hemispheres. The day-to-day changes in tropical convective activity thus seem to be physically linked to the day-to-day changes in the subtropical high cells. This suggests that the secret to the understanding and prediction of changes in monsoon activity on a time scale of days lies in understanding the detailed structure of the subtropical anticyclones.

APPENDIX

Computation of Velocity Potential and Divergent Wind on the Sphere

The procedure used follows that used in preparing vorticity and divergence fields for spectral models. The global FGGE IIIB zonal and meridional (u, v) data on 98 equally spaced latitudes and 192 equally spaced longitudes is interpolated to 56 unequally spaced Gaussian latitudes using a two-dimensional spline under tension. Fourier coefficients are then computed at each latitude circle, and vorticity and divergence spectral coefficients are obtained by evaluating the spectral representations of

$$\xi = \frac{1}{a\cos^2\varphi}\frac{\partial V}{\partial\varphi} - \cos\varphi\frac{\partial U}{\partial\varphi}, \tag{A1}$$

$$D = \frac{1}{a\cos^2\varphi}\frac{\partial U}{\partial\lambda} + \cos\varphi\frac{\partial V}{\partial\varphi}, \tag{A2}$$

where

$$U = u\cos\varphi, \quad V = v\cos\varphi \tag{A3}$$

using Gaussian quadrature with rhomboidal truncation $J = 21$.

The spectral coefficients for the velocity potential χ_l^m are readily obtained from the divergence spectral amplitudes D_l^m as

$$\chi_l^m = \frac{-1}{l(l+1)} D_l^m, \tag{A4}$$

and the spectral coefficients of the components of the divergent wind can then be found from the spectral representation of

$$U_\chi = \frac{1}{a}\frac{\partial\chi}{\partial\varphi}, \tag{A5}$$

$$V_\chi = \frac{\cos\varphi}{a}\frac{\partial\chi}{\partial\varphi}, \tag{A6}$$

which are

$$(U_\chi)_l^m = im\chi_l^m, \tag{A7}$$

$$(V_\chi)_l^m = -\epsilon_l^m(l-1)\chi_{l-1}^m + (l+2)\epsilon_{l+1}^m\chi_{l+1}^m, \tag{A8}$$

where

$$\epsilon_l^m = \left[\frac{(l-m)(l+m)}{(2l+1)(2l-1)}\right]^{1/2}.$$

These various spectral coefficients are then transformed directly to the desired latitude–longitude grid using an expansion such as

$$u(\varphi,\lambda) = \frac{a}{\cos\varphi}\sum_{m=-J}^{J}\sum_{l=|m|}^{|m|+J+1}(U_\chi)_l^m P_l^m(\sin\varphi)e^{im\lambda} \tag{A9}$$

with $J = 21$.

REFERENCES

Chang, C. P., and K. M. Lau, 1982: Short-term planetary-scale interactions over the tropics and midlatitudes during northern winter. Part 1: Contrasts between active and inactive periods. *Mon. Wea. Rev.*, **110**, 933–946.

——, J. E. Erikson and K. M. Lau, 1979: Northeasterly cold surges and near equatorial disturbances over the Winter Monex area during December 1974. Part 1: Synoptic aspects. *Mon. Wea. Rev.*, **107**, 812–829.

Cheang, B. K., 1977: Synoptic features and structures of some equatorial vortices over the South China Sea in the Malaysia region during the winter monsoon, December 1973. *Pure Appl. Geophys.* **115**, 1303–1334.

Daggupaty, S. M., and D. R. Sikka, 1977: On the vorticity budget and vertical velocity distribution associated with the life cycle of a monsoon depression. *J. Atmos. Sci.*, **34**, 773–792.

Davidson, N. E., and B. J. McAvaney, 1981: The ANMRC tropical analysis scheme. *Aust. Meteor. Mag.*, **29**, 155–168.

——, J. L. McBride and B. J. McAvaney, 1983: The onset of the Australian monsoon during Winter Monex: Synoptic aspects. *Mon. Wea. Rev.*, **111**, 496–516.

Holton, J. R., 1972: *An Introduction to Dynamic Meteorology*, Academic Press, 319 pp.

Krishnamurti, T. N., 1968: A diagnostic balance model for studies

of low and high latitudes, Rossby number less than 1. *Mon. Wea. Rev.*, **96,** 197–207.

——, 1971: Tropical east–west circulations during the northern summer. *J. Atmos. Sci.*, **28,** 1342–1347.

——, M. Kanamitsu, W. J. Koss and J. D. Lee, 1973: Tropical east–west circulations during the northern winter. *J. Atmos. Sci.*, **30,** 780–787.

Lau, K. M., and H. Lim, 1982: Thermally driven motions in an equatorial β-plane: Hadley and Walker circulations during the winter monsoon. *Mon. Wea. Rev.*, **110,** 336–353.

Lim, H., and C. P. Chang, 1981: A theory for midlatitude forcing of tropical motions during winter monsoons. *J. Atmos. Sci.*, **38,** 2377–2392.

Lorenz, E. N., 1969: The nature of the global circulation of the atmosphere: A present view. *The Global Circulation of the Atmosphere,* G. A. Corby, Ed., Roy. Meteor. Soc., 3–23.

McBride, J. L., and W. M. Gray, 1980: Mass divergence in tropical weather systems. Part II: Large-scale controls on convection. *Quart. J. Roy. Meteor. Soc.*, **106,** 517–538.

Murakami, T., and A. Sumi, 1982a: Southern Hemisphere summer monsoon circulation during the 1978–79 WMONEX. Part II: Onset, active and break monsoons. *J. Meteor. Soc. Japan,* **60,** 649–670.

——, and ——, 1982b: Southern Hemisphere summer monsoon circulation during the 1978–79 WMONEX. Part I: Monthly mean wind fields. *J. Meteor. Soc. Japan,* **60,** 638–648.

Puri, K., and W. Bourke, 1982: A scheme to retain the Hadley circulation during nonlinear normal mode initialization. *Mon. Wea. Rev.*, **110,** 327–335.

Sangster, W. E., 1960: A method of representing the horizontal pressure force without reduction of pressures to sea level. *J. Meteor.*, **17,** 166–176.

Shukla, J., and K. R. Saha, 1974: Computation of non-divergent streamfunction and irrotational velocity potential from the observed winds. *Mon. Wea. Rev.*, **102,** 419–425.

Webster, P. J., 1981: Cold surges of the winter monsoon: Dynamic structures. *Int. Conf. on Scientific Results of the Monsoon Experiment,* Denpasar, Indonesia, WMO, 2-3 to 2-8.

Williams, M., 1979: Inter-hemispheric interaction during Winter Monex. *Preprints Australia–New Zealand GARP Symp.*, Melbourne, 73–78. [Available from ANMRC, Box 5089AA, Melbourne 3001, Australia.]